

Quantum Artificial Life in an IBM Quantum Computer

U. Alvarez-Rodriguez,^{1,*} M. Sanz,¹ L. Lamata,¹ and E. Solano^{1,2,3}

¹*Department of Physical Chemistry, University of the Basque Country UPV/EHU, Apartado 644, 48080 Bilbao, Spain*

²*IKERBASQUE, Basque Foundation for Science, Maria Diaz de Haro 3, 48013, Bilbao, Spain*

³*Department of Physics, Shanghai University, 200444 Shanghai, People's Republic of China*

(Dated: March 5, 2022)

We present the first experimental realization of a quantum artificial life algorithm in a quantum computer. The quantum biomimetic protocol encodes tailored quantum behaviors belonging to living systems, namely, self-replication, mutation, interaction between individuals, and death, into the cloud quantum computer IBM *ibmqx4*. In this experiment, entanglement spreads throughout generations of individuals, where genuine quantum information features are inherited through genealogical networks. As a pioneering proof-of-principle, experimental data fits the ideal model with accuracy. Thereafter, these and other models of quantum artificial life, for which no classical device may predict its quantum supremacy evolution, can be further explored in novel generations of quantum computers. Quantum biomimetics, quantum machine learning, and quantum artificial intelligence will move forward hand in hand through more elaborate levels of quantum complexity.

Introduction

As described by Deutsch, a quantum computer is a device that intends to fulfill the Deutsch-Church-Turing principle, namely, to efficiently simulate a finitely realizable physical system in the framework of quantum mechanics [1]. In this context, quantum supremacy would be reached when a quantum processor outperforms classical computers realizing a given task. Along these lines, several proposals to achieve quantum supremacy for a variety of quantum algorithms and quantum simulations have been proposed [2–7].

The keyword “quantum” has overflowed the limits to which was initially constrained and, currently, incessantly spreads through the interdisciplinary scientific literature. Indeed, it is a source of inspiration for the breeding extensions of already existing models with their quantum counterparts [8–10]. Besides the appealing intellectual exercise, this hybridization is often motivated by a plausible improvement in the conditions and enhancement in the efficiency of the developed protocols. From all possible ramifications, including quantum machine learning and quantum artificial intelligence, our research in quantum biomimetics is concerned with the design of a framework for quantum algorithms based on the imitation of biological processes, belonging to the macroscopic classical complexity, and brought down by design to the microscopic quantum realm [11–17]. There may not always be a neat analogy between the physical models underlying our protocols and those used to describe real biological systems, but our proposed effective dynamics only partially aims at emulating core aspects of the mimicked process. From a wide perspective in the history of arts and science, close imitation is a natural first layer and wish in the aesthetic process. In this sense, plain simulation is a valid and fruitful engineering playground, where analogies abound and serve as communicating vessels between unconnected fields. Our central goal in quantum simulations and quantum computing is to go beyond it, through a higher creativity challenge, in the search of a second layer of a major art.

In the particular scenario of artificial life, simple models of organisms are able to undergo most common stages of life in a controlled virtual environment [18–20]. When extending this to the quantum realm, particularities of quantum physics, such as its limitation to linear dynamics, the no-cloning theorem, or the exponentially growing dimensionality of Hilbert spaces, play a relevant role. The quantum artificial life protocol we have engineered and implemented goes beyond the straightforward quantization of existing classical models. In this sense, and with similar spirit of other contributions [21–24], it is noteworthy to mention that we leave open the question whether the origin of life is genuinely quantum mechanical. What we prove here is that microscopic quantum systems can efficiently encode quantum features and biological behaviours, usually associated with living systems and natural selection.

In this article, we report the first experimental implementation of a model for quantum artificial life [13] into a quantum computer. To this end, we make use of the facilities provided by the IBM *ibmqx4* quantum computing chip [25]. This work should be aligned with the ramping developments in classical and quantum machine learning and artificial intelligence: the development of algorithms and devices with the capacity to interpret and mimic human behaviors in order to solve useful problems and improve the interaction with human beings. Along these lines, we may

*Electronic address: unaialvarezr@gmail.com

foresee a future in which these idealized machines hybridize the knowledge in machine learning, artificial intelligence, and artificial life, with an internal structure and dynamics following the laws of quantum physics, as is already happening in the classical domain [26].

Results

We begin with a brief description of the model for quantum artificial life [13], whose most important elements are the quantum living units or individuals. Each of them is expressed in terms of two qubits that we call genotype and phenotype. The genotype contains the information describing the type of living unit, an information that is transmitted from generation to generation. The state of the phenotype is determined by two factors: the genetic information and the interaction between the individual and its environment. This state, together with the information it encodes, is degraded during the lifetime of the individual.

The goal of the proposed model is to reproduce the characteristic processes of Darwinian evolution, adapted to the language of quantum algorithms and quantum computing. The self-replication mechanism is based on two partial quantum cloning events, an operation that entangles either the genotype or the phenotype with a blank state and copies a certain expectation value of the original qubit in both of the outcome qubits. In this set of experiments, the self-replication consists in duplicating the expectation value of σ_z in the genotype, in a blank state that will be transformed in the genotype of the individual in the next generation [12]. The process is completed by copying again σ_z of the new genotype in another blank state that will be transformed in the phenotype of the new individual. The next subprotocol in the algorithm is the interaction between the individuals and the environment, which emulates the aging of living units until an asymptotic state that represents its death. This evolution is encoded in a dissipative dynamics that couples a bath with each of the phenotype qubits, with $\sigma = |0\rangle\langle 1|$ as Lindblad operator. The effective lifetime, i.e., the time the phenotype needs to arrive to the dark state of the Lindbladian up to a given error, depends implicitly on the genotype. The protocol also accounts for mutations, performed via random single qubit rotations in the genotype qubits or via errors in the self-replication process [13]. The final ingredient is the interaction between individuals, which conditionally exchange the phenotypes depending on the genotypes [13]. This behavior is achieved via a four-qubit unitary operation, where genotypes and phenotypes play the role of control and target qubits, respectively. The conjunction of these components leads to a minimal but consistent Darwinian quantum scenario. The protocol may be enriched when including spatial information, either quantum or classical, or increasing the model complexity by considering a larger set of observables.

The first step for this implementation is to express each of the building blocks of the previous paragraph in terms of the quantum gates available in the superconducting circuit architecture of IBM cloud quantum computer [25]. Since we have selected σ_z as the observable to clone, every partial quantum cloning event requires the realization of a U_{CNOT} gate, that can be directly performed in the experiment. Regarding the interaction with the environment, we have adapted our protocol, because the experimental device does not allow to realize a conditional projection of the quantum state to the $|0\rangle$ in the phenotypes. The alternative we propose is to implement the transition between the basis states as a sequence of small rotations in σ_y for the phenotype qubits, $e^{-i\sigma_y\theta}$, with θ tuned according to the duration of each simulated time step. This type of rotation can be realized in the experiment via the $u_3(\theta, \phi, \lambda)$ gate,

$$u_3(\theta, \phi, \lambda) = \begin{pmatrix} \cos \frac{\theta}{2} & -e^{i\lambda} \sin \frac{\theta}{2} \\ e^{i\phi} \sin \frac{\theta}{2} & e^{i(\phi+\lambda)} \cos \frac{\theta}{2} \end{pmatrix},$$

with $u_3(\theta, 0, 0)$. The same gate acting on genotype qubits can be used for the mutation events. Ideally, and in order to emulate their randomness both in the phase θ and in the presence or absence of the event, we could design the experimental runs following a classical program. For making the procedure tractable, we could discretize the range of θ in n values, and divide the total experimental runs in $n + 1$ groups to account for each of the different possibilities. The weight, or number of runs for each group, would depend on our selection for the mutation rate as well as on the random parameters obtained with the external program. However, constrained by the flexibility of the experimental device, we propose a less realistic but pragmatic procedure: assume that the mutations will only be of a specific θ , and therefore eliminate a source of randomness and diversity in the protocol. The single-qubit gate accounting for the mutations will be σ_x . Regarding the randomness in the presence or absence of mutation events, we will have to adapt our algorithm to perform the mutations in groups of 1024 experimental runs, and achieve the mutation rate accordingly. The last subprotocol, the inter-individual interactions, requires the implementation of the interaction gate U_I , whose effect is to exchange two pairs of quantum levels, while leaving the rest unaltered, as $U_I|xyyy\rangle = |xyyx\rangle$ and $U_I|xyyx\rangle = |xyyy\rangle$, for $\{x, y\} \in \{0, 1\}$. The challenge is to decompose U_I in terms of the gates offered by the experimental setup. Our solution is given by $U_I = S_{23}U_{12}(\mathbb{1} \otimes F)U_{12}S_{23}$, with $F = U_{43}C_{34}C_{24}U_{23}C_{34}^\dagger U_{43}U_{23}$. Here, the first and second subindices denote the control and target qubit respectively, U is the controlled-not gate, S is the

losing its exponential character. The course of time is simulated by this gate, by implementing one of them for every simulated time step. Subsequently, a second individual is created in a complete self-replication event with two partial quantum cloning operations. To conclude, $u_3(\pi/8, 0, 0)$ is implemented again on both genotypes associated with a next time step. We assign the Hilbert space of the simulating device as $|Q_0Q_1Q_2Q_4\rangle \rightarrow |p_2g_2g_1p_1\rangle$ to maximize the efficiency of the protocol. See Fig. 2 for the quantum circuit diagram. The results, shown in Table II, account for similar probability distributions between the ideal and the real data with a fidelity of 91.18%, as before computed only for the computational basis.

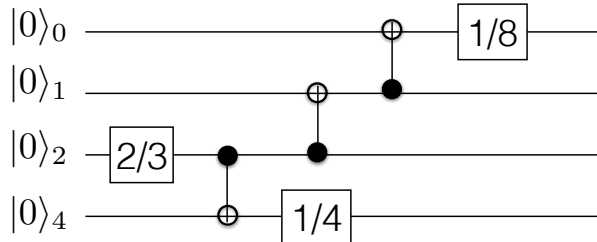


FIG. 2: The initialization of a genotype before three partial quantum cloning events. The first of these will produce an initial individual and the remaining two will replicate it into a second one. The protocol continues with single-qubit gates that emulate the dissipation. The squares denote $U_3(\theta, \phi, \lambda)$ gates where the number indicates the value of θ .

Basis element	0000	0001	0010	0011	0100	0101	0110	0111	1000	1001	1010	1011	1100	1101	1110	1111
Measured events	1491	103	42	224	387	46	31	249	67	91	108	916	149	354	439	3495
Predicted events	1682	66	0	0	288	11	0	0	0	0	34	866	0	0	200	5045

TABLE II: **Self-replication and interaction with the environment in the σ_z basis.** Number of measurements for every element of the four-qubit basis. The experimental values for $\langle \sigma_z \rangle$ are $(-0.37, -0.26, -0.34, -0.34)$ while the ideal values are $(-0.5, -0.35, -0.5, -0.46)$. Notice that the mapping of reordering the qubits has been inverted to achieve the results in the $|g_1p_1g_2p_2\rangle$ basis.

For the self-replication instance, there is an additional property of the model that only arises when measuring some purely quantum correlations of the system. The partial quantum cloning operation entangles the qubits which are involved on it, transmitting $\langle \sigma_x \rangle$ of the original state into $\langle \sigma_x \otimes \sigma_x \rangle$. Note that this data can be extracted from the experiment when measuring on the σ_x basis, which is done by introducing a Hadamard gate in every entry before projecting. Therefore, one has to compute $\langle \sigma_z \otimes \sigma_z \otimes \sigma_z \otimes \sigma_z \rangle$ in the new basis, to retrieve $\langle \sigma_x \otimes \sigma_x \otimes \sigma_x \otimes \sigma_x \rangle$. This technique is based on the equality $\text{Tr}[\sigma_x \rho] = \text{Tr}[\sigma_z H \rho H]$, since $\sigma_x = H \sigma_z H$. Even if the calculation for the fidelity yields a satisfactory 93.45%, the value of $\langle \sigma_x \otimes \sigma_x \otimes \sigma_x \otimes \sigma_x \rangle$ still shows a sizable error with respect to the ideal one, as we show in Table III.

Basis element	0000	0001	0010	0011	0100	0101	0110	0111	1000	1001	1010	1011	1100	1101	1110	1111
Measured events	753	246	277	52	448	747	569	513	343	493	616	177	717	679	345	749
Predicted events	624	1	77	547	157	1150	704	603	77	547	624	1	704	603	157	1150

TABLE III: **Self-replication and interaction with the environment in the σ_x basis.** Number of measurements for every element of the four-qubit basis rotated to σ_x . The experimental value for $\langle \sigma_x \otimes \sigma_x \otimes \sigma_x \otimes \sigma_x \rangle$ is 0.22 while the ideal value is 0.56. Again, the qubits have been reordered to coincide with the ideal results in the $|g_1p_1g_2p_2\rangle$ basis.

The implementation of mutations requires to combine the outcome of different designs of quantum circuit diagrams and, therefore, experimental runs. In this case, we consider that a mutation event, which can affect both individuals, is simulated with a σ_x . The complete result is achieved when gathering data from 4 different groups of experiments, that correspond to the cases of mutation on the first genotype, mutation on the second genotype, mutation on both genotypes, and no mutation. We have performed 1024 experimental runs for each of the three cases with mutations and 8192 runs for the no-mutation rate. These results have been combined with the ones shown in Table II, that coincide with the no-mutation case, with the goal of reducing the mutation rate for each individual, which takes a

final value of $2/19$. See Table IV for the measured data with a fidelity of 94.86% with respect to the ideal case in the σ_z basis.

Basis element	0000	0001	0010	0011	0100	0101	0110	0111	1000	1001	1010	1011	1100	1101	1110	1111
Measured events	3201	282	385	447	1344	217	541	494	235	608	297	2026	464	1509	946	6325
Predicted events	3466	137	309	12	1174	46	622	25	12	303	76	1930	26	659	401	10123

TABLE IV: **Self-replication, interaction with the environment and mutations.** Number of measurements for every element of the four-qubit basis rotated to σ_x . The experimental values for $\langle \sigma_z \rangle$ are $(-0.28, -0.23, -0.19, -0.23)$ while the ideal values are $(-0.40, -0.35, -0.40, -0.37)$. The experimental basis is also permuted to coincide with the ideal results in the $|g_1 p_1 g_2 p_2\rangle$ basis.

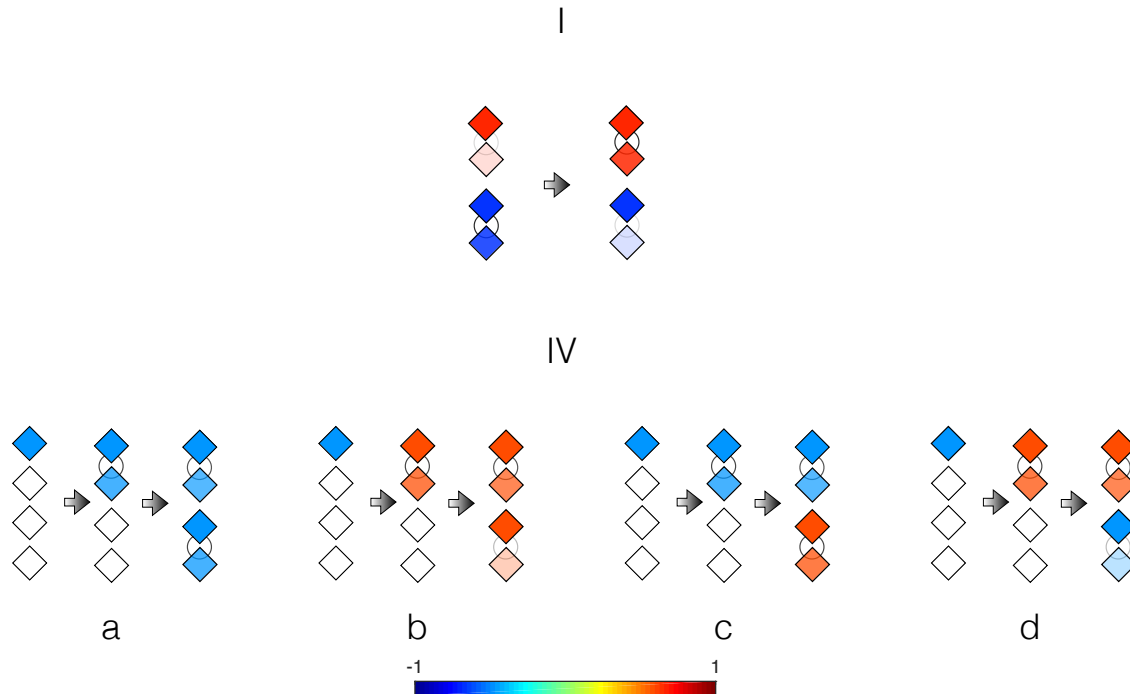


FIG. 3: Visualization of the ideal processes in experiments I and IV. We depict the individuals as combinations of two diamonds that represent the genotype and phenotype qubits. The color in the genotype qubit, the upper diamond of each pair, depends on the value of σ_z as indicated in the color bar. The color in the phenotype qubit is the same as in the genotype one, as the color is meant to be showing the genetic information. Moreover, the opacity of this color is modified according to the expectation value of σ_z being limited by the value of 1 that corresponds to the blank qubits. In both cases the right arrow separates two consecutive time steps. Following these clarifications, we can see the exchange of phenotypes in I, and the self-replication followed by different mutation possibilities in IV.

Realization of the complete model of quantum artificial life. The last round of experiments is devoted to the reproduction of the aggregate of properties in the quantum artificial life algorithm. In order to maintain the fidelity in values that allow us to claim that the experiment is indeed behaving according to the protocol, we restrict our analysis to the case of two interacting individuals, which undergo mutations and dissipation. Then, the quantum circuit diagram, shown in Fig. 4, is an upgraded version of the one shown in Fig. 1 that includes $u_3(\pi/8, 0, 0)$ for simulating the dissipation in the phenotypes. For the mutations, we follow the same strategy as in the previous subsection, combining the data generated with different quantum circuit diagrams each of them emulating a specific case of the presence or absence of mutation instances. In particular, 3 rounds of 8192 runs emulating the no-mutation case and 1024 runs for each of the mutation cases determine a mutation rate of $2/27$. The post-processing of the data, in Table V, matches the ideal probability distribution in the computational basis with a fidelity of 93.94%.

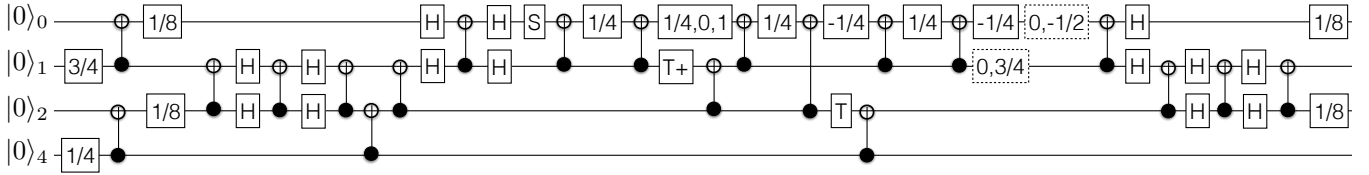


FIG. 4: Quantum circuit diagram for the complete quantum artificial life protocol. The squares with dashed and solid lines represent $u_2(\phi, \lambda)$ and $u_3(\theta, \phi, \lambda)$ single-qubit gates, respectively. The rotation angles are expressed in radians.

Basis element	0000	0001	0010	0011	0100	0101	0110	0111	1000	1001	1010	1011	1100	1101	1110	1111
Measured events	3449	1598	2656	2053	2361	298	6369	2166	521	500	629	529	594	692	656	1146
Predicted events	2221	924	2221	410	410	251	12401	2207	237	410	237	838	584	251	410	2207

TABLE V: **Complete model.** Number of measurements for every element of the four-qubit basis rotated to σ_x . The experimental values for $\langle \sigma_z \rangle$ are (0.60, -0.09, -0.24, 0.31) while the ideal values are (0.60, -0.43, -0.60, 0.43). The experimental basis is also permuted to coincide with the ideal results in the $|g_1 p_1 g_2 p_2\rangle$ basis.

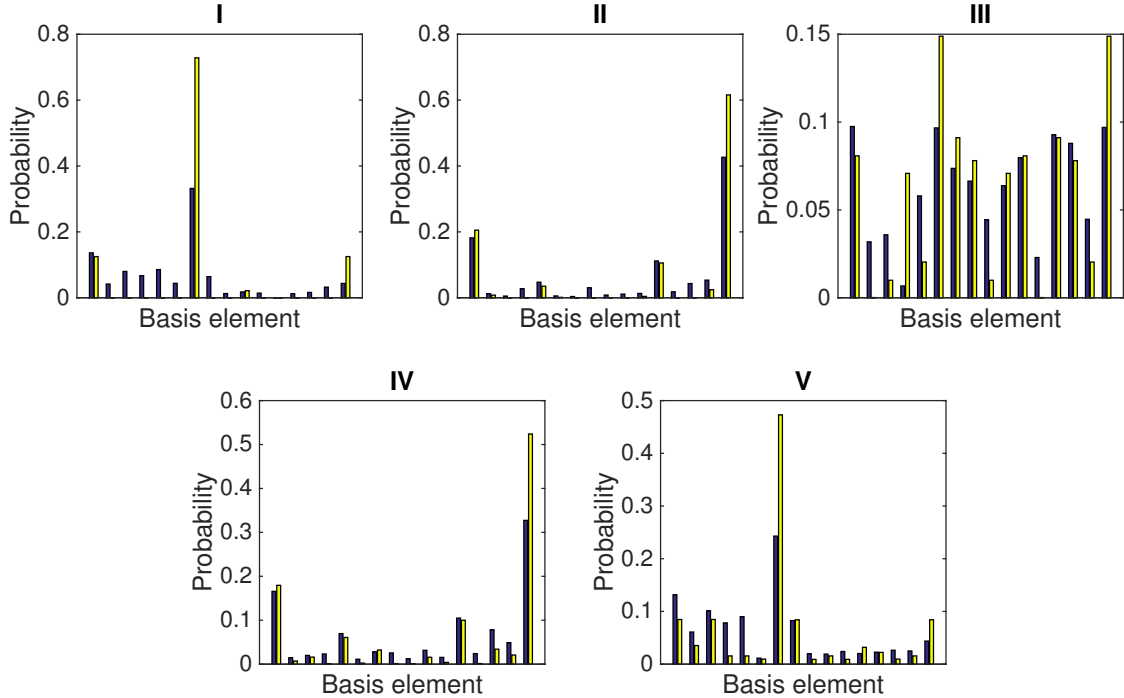


FIG. 5: Experimental and ideal probability distributions for all the cases analyzed. In each pair of columns the blue one in the left denotes the experimental value while the yellow one in the right denotes the ideal estimation. The labels in the subplots correspond to the tables for the different quantum artificial life instances.

Discussion

Regarding errors in the experimental protocol, even if the fidelities achieved are satisfactory, they do not correspond to the fidelities of the complete quantum state. In this sense, the prediction for the number of events to measure is done by simply multiplying the probability distribution by the number of events. These do not exactly match the experimental data (see Table VI for all experimental outcomes). Indeed, the distances have to be properly weighed,

since the probability distribution is the key quantity to be extracted (see Fig. 5). Moreover, the overlap between expectation values of observables in the measurement basis is lower than the fidelity of the probability distribution for all cases analyzed here.

	0000	0001	0010	0011	0100	0101	0110	0111	1000	1001	1010	1011	1100	1101	1110	1111
I	1104	338	647	542	693	355	2687	519	104	144	114	1	99	132	261	353
II	1491	103	42	224	387	46	31	249	67	91	108	916	149	354	439	3495
III	753	246	277	52	448	747	569	513	343	493	616	177	717	679	345	749
IVa	1511	121	46	201	395	86	27	213	102	192	162	984	215	635	478	2824
IVb	136	14	3	14	542	32	9	6	12	29	16	122	17	12	1	5
IVc	39	28	149	7	13	34	46	3	22	137	6	2	68	444	16	1
IVd	24	16	145	1	7	19	428	23	32	159	5	2	15	64	12	0
Va	1032	422	756	594	737	51	2121	731	88	109	132	113	99	179	186	383
Vb	1087	414	863	696	697	44	2076	692	107	107	134	97	99	191	188	304
Vc	1046	445	871	631	723	46	2056	634	111	114	154	148	97	162	192	348
Vd	7	6	48	45	47	5	24	61	99	89	119	122	39	48	35	68
Ve	219	269	62	63	74	87	44	27	27	15	15	7	28	57	12	18
Vf	58	42	56	24	83	65	48	21	89	66	75	42	232	55	43	25

TABLE VI: **Experimental data.** The rows denote the number of events in each of the elements of the computational basis for all the instances considered. For the composite experiments, in order to retrieve the measurements shown in previous tables, one has to add all the events in each of the individual runs. In the particular case of IV, the data in II also contributes to the final result.

In parallel, the assignment between the simulated and the simulating Hilbert spaces is designed to maximize the fidelity according to the calibration parameters provided by IBM. Nevertheless, the recalibration of the circuit changes the gate and readout errors, so we reevaluate our circuit according to the new parameters and adapt it when the fidelity outcome can be improved with a different labeling of qubits. Consequently, the performance of the different experiments is not directly comparable, since they have been implemented under unequal conditions.

Despite the different factors degrading the implementation, the performed experiments reproduce the characteristic properties of the sought quantum natural selection scenario. We have observed how the partial quantum cloning events allow us to inherit the information of $\langle \sigma_z \rangle$ from qubit to qubit, and use this property to encode the self-replication process. We have also seen how nonzero quantum correlations assure that both individuals have been part of a same event in their timelines, in this case self-replication. Another relevant characteristic of the analysis is the inclusion of mutations as a source of randomness that, counterintuitively, significantly improved the fidelity of the quantum algorithm outcome. Our explanation is that mutations tend to homogenize the probability distribution, which is the same effect as the one produced by the errors naturally present in the experimental platform. Surprisingly, in the classical realm, mutations also help the species to adapt to changing environments.

This experimental realization of the proposed quantum algorithm represents the consolidation of the theoretical framework of quantum artificial life. The improvement in scalable quantum computers will soon allow us for more accurate quantum emulations with growing complexity towards quantum supremacy, even considering spatial variables for the individuals and a mechanism for tracing out death living units. These future developments should lead towards an autonomous character of the set of individuals, i.e., the evolution will be an intrinsic property of the system, and the desired behavior will emerge without following the instructions of a previously designed quantum algorithm. In this context, the system would be transformed into an intelligent source of quantum complexity whose evolutionary plot for a large number of individuals may not be predicted classically and, consequently, has the capacity to produce unexpected results when scaled up. An interesting question to address is to establish the relation existing between the parameters defining the fundamental processes of the model, and the emergent multiqubit quantum state. Along these lines, and following the frame of artificial life oriented genetic algorithms [28], we speculate about the idea of channeling this complexity to encode optimization problems by tuning the self-replication, mutation and dissipation rates that define the evolution. Furthermore, recent advances in quantum machine learning constitute a promising material to work with in the study of algorithms combining the properties of both fields, pursuing the design of intelligent and replicating quantum agents. Therefore, the creation of these quantum living units and their possible applications are expected to have deep implications in the community of quantum simulation and quantum computing in a variety of quantum platforms.

All in all, the experiments presented here entail the validation of quantum artificial life in the lab and, in particular, in cloud quantum computers as that of IBM. Still another interesting step would be the development of autonomous

quantum devices following the theoretical and experimental results in quantum cellular automata [29, 30]. Our quantum individuals are driven by an adaptation effort along the lines of a quantum Darwinian evolution, which effectively transfer the quantum information through generations of larger multiqubit entangled states. We believe that the presented results and vision, both in theory and experiments, should hoist this innovative research line as one of the leading banners in the future of quantum technologies.

-
- [1] D. Deutsch, Quantum theory, the Church-Turing principle and the universal quantum computer, *Proc. Roy. Soc. London A* **400**, 97 (1985).
- [2] R. P. Feynman, Simulating physics with computers, *Int. J. Theor. Phys.* **21**, 467 (1982).
- [3] D. Deutsch and R. Jozsa, Rapid solutions of problems by quantum computation, *Proc. Roy. Soc. London A* **439**, 553 (1992).
- [4] L. K. Grover, A fast quantum mechanical algorithm for database search, *Proceedings, 28th Annual ACM Symposium on the Theory of Computing (STOC)* 212 (1996).
- [5] S. Lloyd, Universal quantum simulators, *Science* **273**, 1073 (1996).
- [6] P. W. Shor, Polynomial time algorithms for prime factorization and discrete logarithms on a quantum computer, *SIAM J. Sci. Statist. Comput.* **26**, 1484 (1997).
- [7] S. Aaronson and A. Arkhipov, The Computational Complexity of Linear Optics, *Proceedings, 43rd Annual AMC Symposium on the Theory of Computing (STOC)* 333 (2011).
- [8] S. Wiesner, Conjugate coding, *SIGACT News* **15** 78, (1983); C. H. Bennett and G. Brassard, Quantum cryptography: Public key distribution and coin tossing. In Proceedings of IEEE International Conference on Computers, Systems and Signal Processing, volume 175, page 8. New York, 1984; A. K. Ekert, Quantum cryptography based on Bells theorem, *Phys. Rev. Lett.* **67**, 661 (1991).
- [9] Y. Aharonov, L. Davidovich, and N. Zagury, Quantum random walks, *Phys. Rev. A* **48**, 1687 (1993); N. Shenvi, J. Kempe, and K. B. Whaley, Quantum random-walk search algorithm, *Phys. Rev. A* **67**, 052307 (2003).
- [10] J. Biamonte, P. Wittek, N. Pancotti, P. Rebentrost, N. Wiebe, and S. Lloyd, Quantum machine learning, *Nature* **549**, 195 (2017); V. Dunjko and H. J. Briegel, Machine learning & artificial intelligence in the quantum domain, arXiv:1709.02779 (2017); M. Schuld, I. Sinayskiy, and F. Petruccione, An introduction to quantum machine learning, *Contemporary Phys.* **56**, 172 (2014); U. Alvarez-Rodriguez, L. Lamata, P. Escandell-Montero, J. D. Martín-Guerrero, and E. Solano, Supervised Quantum Learning without Measurements, *Scientific Reports* **7**, 13645 (2017); L. Lamata, Basic protocols in quantum reinforcement learning with superconducting circuits, *Scientific Reports* **7**, 1609 (2017).
- [11] E. Schrödinger, *What is life?* (Cambridge University Press, Cambridge, UK, 1944).
- [12] U. Alvarez-Rodriguez, M. Sanz, L. Lamata, and E. Solano, Biomimetic Cloning of Quantum Observables, *Scientific Reports* **4**, 4910 (2014).
- [13] U. Alvarez-Rodriguez, M. Sanz, L. Lamata, and E. Solano, Artificial Life in Quantum Technologies, *Scientific Reports* **6**, 20956 (2016).
- [14] U. Alvarez-Rodriguez, R. Di Candia, J. Casanova, M. Sanz, and E. Solano, Algorithmic quantum simulation of memory effects, *Phys. Rev. A* **95**, 020301 (2017) ; U. Alvarez-Rodriguez, A. Perez-Leija, I. L. Egusquiza, M. Gräfe, M. Sanz, L. Lamata, A. Szameit, and E. Solano, Advanced-Retarded Differential Equations in Quantum Photonic Systems, *Scientific Reports* **7**, 42933 (2017).
- [15] U. Las Heras, U. Alvarez-Rodriguez, E. Solano, and M. Sanz, Genetic Algorithms for Digital Quantum Simulations, *Phys. Rev. Lett.* **116**, 230504 (2016).
- [16] P. Pfeiffer, I. L. Egusquiza, M. Di Ventra, M. Sanz, and E. Solano, Quantum Memristors, *Scientific Reports* **6**, 29507 (2016).
- [17] J. Salmilehto, F. Deppe, M. Di Ventra, M. Sanz, and E. Solano, Quantum Memristors with Superconducting Circuits, *Scientific Reports* **7**, 42044 (2017); M. Sanz, L. Lamata, and E. Solano, Quantum Memristors in Quantum Photonics. arXiv:1709.07808 (2017).
- [18] C. G. Langton, *Artificial Life: An overview* (MIT Press, Cambridge USA, 1997).
- [19] M. Gardner, The fantastic combinations of John Conway's new solitaire game life, *Sci. Am.* **223**, 120 (1970).
- [20] T. S. Ray, Ecology and Optimization of Digital Organisms. Santa Fe Institute (1992). Available at: <http://samo.santafe.edu/media/workingpapers/92-08-042.pdf> (Accessed: 10th October 2017).
- [21] M. A. Martin-Delgado, On Quantum Effects in a Theory of Biological Evolution, *Sci. Rep.* **2**, 302 (2012).
- [22] D. Abbott, P. C. W. Davies, and A. K. Pati, *Quantum Aspects of Life* (Imperial College Press, London, 2008).
- [23] P. Arrighi and J. Grattage, A Quantum Game of Life. Paper presented at Journées Automates Cellulaires, Turku, Finland (2010, December 15).
- [24] D. Bleh, T. Calarco, and S. Montangero, Quantum Game of Life. *EPL* **97**, 20012 (2012).
- [25] IBM Quantum Experience, <https://www.research.ibm.com/ibm-q/> (last accessed 10 October 2017).
- [26] L. Steels, The Artificial Life Roots of Artificial Intelligence, *Artif. Life* **1**, 75 (1994).
- [27] M. A. Nielsen and I. L. Chuang, *Quantum Computation and Quantum Information* (Cambridge University Press, Cambridge, UK, 2000).
- [28] M. Mitchell and S. Forrest, Genetic Algorithms and Artificial Life, *Artif. Life* **1**, 267 (1994).

- [29] C. S. Lent, P. D. Tougaw, W. Porod, and G. H. Bernstein, Quantum cellular automata, *Nanotechnology*, **4**, 1 (1993).
- [30] A. O. Orlov, I. Amlani, G. H. Bernstein, C. S. Lent, and G. L. Snider, Realization of a Functional Cell for Quantum-Dot Cellular Automata, *Science* **277**, 928 (1997); I. Amlani, A. O. Orlov, G. Toth, G. H. Bernstein, C. S. Lent, and G. L. Snider, Digital Logic Gate Using Quantum-Dot Cellular Automata, *Science* **284**, 289 (1999); R. P. Cowburn and M. E. Welland, Room Temperature Magnetic Quantum Cellular Automata, *Science* **287**, 1466 (2000); A. Imre, G. Csaba, L. Ji, A. Orlov, G. H. Bernstein, and W. Porod, Majority Logic Gate for Magnetic Quantum-Dot Cellular Automata, *Science* **311**, 205 (2006).

Acknowledgements

We thank Armando Pérez-Leija and Alexander Szameit for enthusiastic and enlightening discussions. We acknowledge the use of IBM Quantum Experience for this work. The views expressed are those of the authors and do not reflect the official policy or position of IBM or the IBM Quantum Experience team. We acknowledge support from Spanish MINECO/FEDER FIS2015-69983-P, UPV/EHU new PhD program, Basque Government IT986-16, and Ramón y Cajal Grant RYC-2012-11391.

Author Contributions

U. A.-R. performed the experiments on the IBM Quantum Experience. U. A.-R., M. S., L. L., and E. S. developed the model and analyzed the data. All authors contributed to writing the manuscript.

Additional Information

Competing financial interests: The authors declare no competing financial interests.